



Article

Quantifying Forest Litter Fuel Moisture Content with Terrestrial Laser Scanning

Jonathan L. Batchelor ^{1,*} , Eric Rowell ², Susan Prichard ¹ , Deborah Nemens ³, James Cronan ³,
Maureen C. Kennedy ⁴ and L. Monika Moskal ¹

¹ School of Environmental and Forest Sciences, University of Washington, Anderson Hall, P.O. Box 352100, Seattle, WA 98195, USA

² Desert Research Institute, 7010 Dandini Blvd, Reno, NV 89512, USA

³ Pacific Wildland Fire Sciences Laboratory, 400 N 34th St., Suite 201, Seattle, WA 98103, USA

⁴ School of Interdisciplinary Arts and Sciences, University of Washington, 1900 Commerce Street, Tacoma, WA 98402, USA

* Correspondence: jonbatch@uw.edu

Abstract: Electromagnetic radiation at 1550 nm is highly absorbed by water and offers a novel way to collect fuel moisture data, along with 3D structures of wildland fuels/vegetation, using lidar. Two terrestrial laser scanning (TLS) units (FARO s350 (phase shift, PS) and RIEGL vz-2000 (time of flight, TOF)) were assessed in a series of laboratory experiments to determine if lidar can be used to estimate the moisture content of dead forest litter. Samples consisted of two control materials, the angle and position of which could be manipulated (pine boards and cheesecloth), and four single-species forest litter types (Douglas-fir needles, ponderosa pine needles, longleaf pine needles, and southern red oak leaves). Sixteen sample trays of each material were soaked overnight, then allowed to air dry with scanning taking place at 1 h, 2 h, 4 h, 8 h, 12 h, and then in 12 h increments until the samples reached equilibrium moisture content with the ambient relative humidity. The samples were then oven-dried for a final scanning and weighing. The spectral reflectance values of each material were also recorded over the same drying intervals using a field spectrometer. There was a strong correlation between the intensity and standard deviation of intensity per sample tray and the moisture content of the dead leaf litter. A multiple linear regression model with a break at 100% gravimetric moisture content produced the best model with R² values as high as 0.97. This strong relationship was observed with both the TOF and PS lidar units. At fuel moisture contents greater than 100% gravimetric water content, the correlation between the pulse intensity values recorded by both scanners and the fuel moisture content was the strongest. The relationship deteriorated with distance, with the TOF scanner maintaining a stronger relationship at distance than the PS scanner. Our results demonstrate that lidar can be used to detect and quantify fuel moisture across a range of forest litter types. Based on our findings, lidar may be used to quantify fuel moisture levels in near real-time and could be used to create spatial maps of wildland fuel moisture content.

Keywords: terrestrial lidar; TLS; fire; wildland fuel; fuel moisture; spectrometer; water content



Citation: Batchelor, J.L.; Rowell, E.; Prichard, S.; Nemens, D.; Cronan, J.; Kennedy, M.C.; Moskal, L.M. Quantifying Forest Litter Fuel Moisture Content with Terrestrial Laser Scanning. *Remote Sens.* **2023**, *15*, 1482. <https://doi.org/10.3390/rs15061482>

Academic Editors: Aqil Tariq and Na Zhao

Received: 28 January 2023

Revised: 25 February 2023

Accepted: 1 March 2023

Published: 7 March 2023



Copyright: © 2023 by the authors. Licensee MDPI, Basel, Switzerland. This article is an open access article distributed under the terms and conditions of the Creative Commons Attribution (CC BY) license (<https://creativecommons.org/licenses/by/4.0/>).

1. Introduction

Water content within live and dead plant material, termed fuel moisture, is one of the most critical contributors to wildland fire behavior. Moisture content determines the availability and likelihood of wildland fuels to ignite and is a driver for many elements of fire behavior including the rate of spread, fireline intensity, and flame length [1,2]. Prior to ignition, moisture must first effectively be boiled off from fuels for fuel temperatures to rise above 200 °C and attain heat for ignition for pyrolysis [3,4]. Live and dead fuel moisture is highly dynamic over space and time and is difficult to measure in diverse fuel types, and at differing spatial and temporal scales. Small changes in solar radiation and weather impact fuel moisture [5] with fuel moisture levels in fine fuels varying throughout the day

depending on the time and temperature [6,7]. Live and coarse dead fuels are minimally affected by daily variations. They respond to longer-term, monthly to seasonal fluctuations in weather and climate [8–10]. Identifying techniques to increase the speed and spatial resolution of fuel moisture measurements has gained importance because fire behavior models increasingly rely on complex data that include the fine-scale characterization of the location and moisture content of potential fuels [11]. With longer and more severe wildfire seasons associated with climate change, real-time assessments of fuel moisture and when fuels are cured for burning are increasingly needed [6,12,13]. Accurate estimates of live and dead fuel moisture are a critical input for fire behavior models, with small variations in fuel moisture levels having a greater effect on model outputs as models become more advanced [7,14].

Fuel moisture estimates can be made at local scales using field sampling techniques or across landscapes with remote sensing techniques. Direct measurement methods can be labor-intensive and time-consuming for a robust quantification. Samples must be collected of either live or dead vegetation and placed in a sealed container to avoid fluctuations caused by changes in ambient relative humidity. Field-collected samples are then oven-dried to ensure that all water is removed from a sample prior to measuring the dry biomass [15]. To calculate gravimetric fuel moisture, the dry weight of the sample is subtracted from the original weight of the sample, and this value is then divided by the dry weight of the sample, following 24–72 h of drying (depending on the size of the fuel element). Due to the need for laboratory processing, such measures of fuel moisture do not produce results until long after the field collection is complete. Another field method used to measure fuel moisture involves the placement of wooden dowels of a known dry weight in the field until the dowels have reached equilibrium with ambient humidity (typically after 12 h). The dowels can then be weighed on-site to determine the moisture content [16]. Electronic fuel moisture probes are also often used to collect moisture estimates digitally [5,15]. However, both methods are limited to a single-point assessment of moisture, and can miss important fuel moisture gradients across space and time. Aggregation of multiple single-point moisture measurements is possible and can be conducted to estimate moisture content across an area, but is cumbersome to implement. A better solution is to employ remote sensing techniques, such that large areas can be accurately sampled in a continuous manner.

1.1. Remote Sensing of Moisture

Remote sensing techniques for quantifying fuel moisture generally rely on the reflectance of the vegetation in sections of the electromagnetic spectrum that are more sensitive to changes in moisture content. The near-infrared (NIR) wavelength 1450 nm and shortwave infrared (SWIR) wavelength 1900 nm are highly absorbed by water. Previous studies have demonstrated that, in these wavelengths, the reflectance of an object will increase as moisture content decreases [17–21]. As a material dries, the relative increase in reflectance will fluctuate with the EM wavelength, but for many plant species the relative change in reflectance is greatest between 1400 nm to 1600 nm (Figure 1). Spectral indices such as the global vegetation moisture index (GVMI) take advantage of this relationship and can be employed using data from numerous remote sensing satellites such as Landsat, MODIS, and Sentinel [17]. Analysis of spectral signatures to quantify fuel moisture content is not limited to landscape-level satellite imagery. Fine-scale spectroscopy has also been used to quantify moisture content in various applications. Examples include determining the influence of moisture content on the combustion and consumption of Douglas-fir (*Pseudotsuga menziesii*) wood samples [22], seasonal variation of moisture content in lodgepole pine (*Pinus contorta*) and big sagebrush (*Artemisia tridentata* Nutt) litter [23], and in lumber mills to sort wood products based on dryness [24]. When viewed with an infrared (IR) camera, dead vegetation that is fully saturated with water appears darker and more heterogeneous than dry vegetation, which appears lighter and more homogenous (Figure 2). Infrared imagery acquired via drone has been shown to have moderate predictive power to

characterize fuel moisture gradients as the radiance of ground cover picked up by a passive IR sensor increases as the material dries [25].

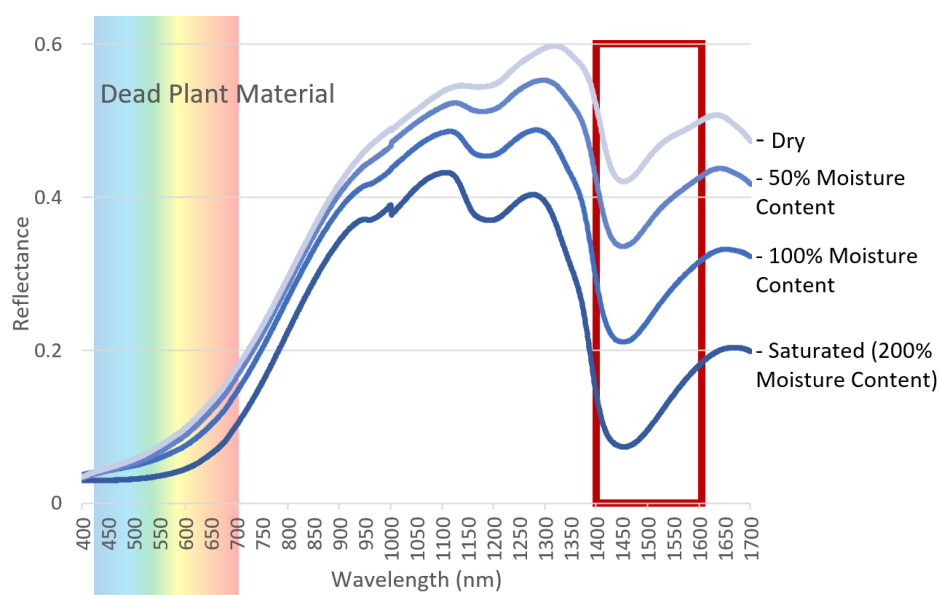


Figure 1. Conceptual diagram of the reflectance of dead vegetation when it is fully saturated with water to when it is dry. The red box is the section of the NIR electromagnetic spectrum that has the greatest change as vegetation dries (1400–1600 nm).

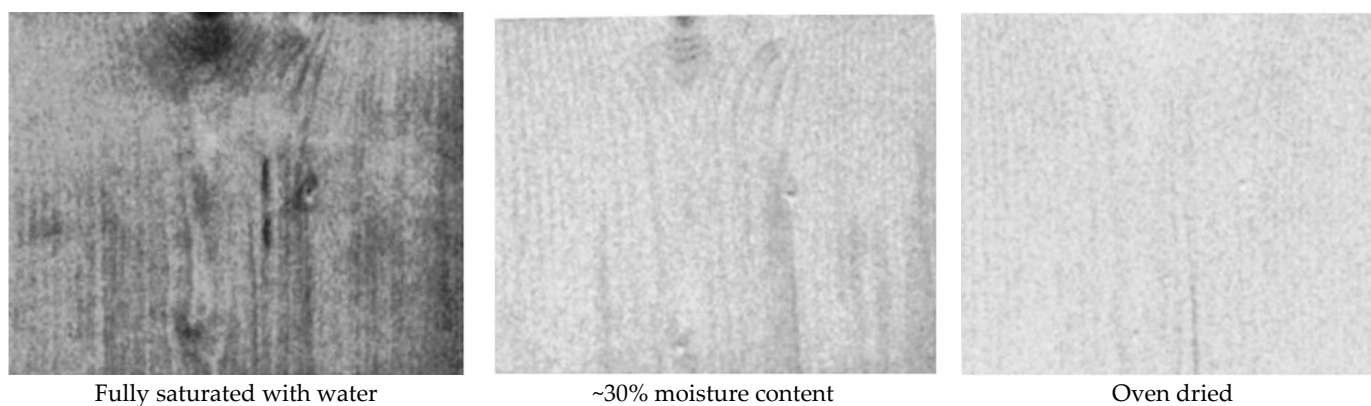


Figure 2. Using a 1550 nm wavelength scanner, scans were taken of a single section of cut pine board fully saturated with water, at approximately 30% moisture content, and oven-dried. When fully saturated, the board not only reflects less light, but reflectance is also more heterogenous across the surface.

1.2. Passive vs. Active Sensors

Passive sensors rely on reflected energy from a controlled external light source or the Sun and have been frequently used to quantify moisture content. This includes the use of satellite imagery for surface and soil water detection [26,27], landscape-scale fuel moisture content quantification [28,29], and spectroscopy for single-sample vegetation moisture content [23,30]. The capacity of active sensors such as light detection and ranging (lidar) sensors to evaluate the moisture content of dead wildland fuels has not been fully evaluated. This evaluation is worthwhile because active sensors offer distinct advantages over passive sensors. Passive sensors are only able to capture the reflectance of the surface of vegetation, while active sensor energy pulses can penetrate through small gaps in the vegetation coverage to sample surfaces that would be occluded to a passive sensor. Further, with active sensors, a three-dimensional (3D) location is also included with each pulse,

while most applications for passive sensors only supply a two-dimensional location. This allows for a 3D model to be made to quantify vegetation structure, as well as a conditional element (moisture content).

A lidar unit sends out a pulse of energy and calculates the distance traveled by each pulse along with the amount (i.e., intensity) of energy returned. A common wavelength for lidar to use is 1550 nm, which is within the NIR section that has a relatively large change in reflectance as a material loses moisture (Figure 1). A large portion of lidar data is collected from aircraft (i.e., airborne laser scanning (ALS)) data and is used to create fine-scale terrain models from the 3D location information from each lidar return. Moisture content estimates across an area have been derived using topographic models derived from lidar [31], but lidar applications extend far beyond ground topography. ALS data have been used extensively to model 3D forest structure elements such as tree height, diameter, and the vertical composition of forest stands, and to identify canopy gaps [32–35]. Vertical point distributions of lidar returns have also been used to model fuel connectivity to characterize fire behavior [36].

The three dimensional point clouds of ALS returns have been used successfully to quantify a multitude of forest structural parameters, and the recorded intensity values have also been used to detect inundated areas (i.e., wetlands), identify tree species from crown architecture, and detect snags [37–39]. ALS has received attention for its potential to quantify surface moisture, but variations in the vegetation cover have contributed more to changes in intensity than the presence of water has [40]. There are inherent issues with using lidar intensity values to quantify ground cover conditions. The amount of energy returned to a scanner depends on the distance traveled, the angle of incidence when contacting a surface, the material of the surface, and the texture of the surface [41]. There is an important distinction between intensity and reflectance. Intensity is the amount of energy returned to the scanner, while reflectance is an objective measurement of what proportion of incoming energy is being reflected from a surface. Reflectance can be modeled from intensity if adjustments are made for the distance traveled, angle of incidence, and surface characteristics. However, calibrating intensity values to derive reflectance is often done by simply adjusting for the distance traveled but not accounting for the angle of incidence or surface texture [42,43]. Further, intensity values are difficult to normalize across the full extent of an acquisition and are typically not calibrated between acquisitions. Intensity maximum thresholds are variable to preclude signal saturation by using automatic gain control. However, if lidar intensity values are normalized, and either a single scanner is used or values are calibrated between scanners, useful spectral information can be derived from intensity values. This would allow for the benefits of active sensors to be combined with spectral reflectance indices to quantify condition information about the vegetation being sampled (i.e., to determine moisture content). Landscape-level ALS is invaluable for forest applications, but are not useful for fuel moisture mapping because ALS flights are costly and generally occur every 1–5 years, whereas fuel moisture can meaningfully change on an hourly to monthly basis depending on the fuel category. Terrestrial laser scanning (TLS) offers an option for fine scale models of fuel moisture to be produced on demand.

1.3. Terrestrial Laser Scanning (TLS)

TLS has been used extensively for the fine-scale modeling of forest structural elements. Using TLS to quantify the location and amount of potential wildfire fuels is a topic that has been extensively researched [44–46]. However, using TLS intensity returns to characterize the condition of wildland fuels has not been fully explored. For a TLS unit using 1550 nm laser light, the amount of energy from a TLS pulse that is reflected off a surface should decrease due to the absorption of energy as surface moisture increases. Just as IR radiation at 1550 nm from the Sun is absorbed, and not reflected, by water vapor and thin layers of water, the same principle holds true for IR radiation generated by a laser [47,48]. For example, TLS has been used to detect moisture in building materials and mapping moisture movement in buildings by comparing relative changes in intensity values of returns [49,50].

Similarly, phase-based TLS units have been successfully used to quantify surface moisture levels on a sandy beach [51].

Intensity values of TLS sensors have been used to quantify many different variables of interest in live vegetation. Much the same as how vegetation spectral indices from images (such as NDVI) can be used to quantify vegetation health, leveraging relationships between different laser wavelengths of TLS units can also provide information on live leaf health and location. Lidar sensors of differing laser wavelengths can be used in conjunction with each other to provide an index based on intensity values to more easily separate leaves from stems [52–54]. TLS intensity values have also been used to quantify the moisture content of live leaves, using a dual wavelength approach to provide an index value [55–58]. Such an approach has been effective at allowing the robust measurement of leaf water content and has been related to overall plant health. Such an approach has also been used to measure fluctuations in leaf water potential on an hourly basis [59], and to model whole-tree fuel moisture content and equivalent water thickness in a three dimensional manner [60,61]. TLS intensity values and specifically the TLS intensity values of two differing wavelengths are proven tools for quantifying moisture content within live vegetation. Many of the studies that use TLS intensity to quantify moisture content provide a calibrated intensity value that accounts for the distance traveled by the laser pulse to attempt to report the reflectance of the surface and not just the amount of energy returned to the scanner (i.e., intensity). TLS intensity value degradation with distance often does not follow a simple linear relationship and some scanners may create a dampening effect to close returns to avoid signal saturation [62,63]. While TLS intensity values have been shown to be related to moisture content on many different levels, leveraging this relationship to quantify moisture gradients in dead forest litter from a single vantage point has yet to be fully explored.

There are a wide range of lidar units that are commonly used for terrain and vegetation mapping. Two significant differences among TLS units are the wavelengths used and how distances are calculated. For this study, we used 1550 nm wavelength terrestrial lidar scanners because of the sensitivity of that wavelength to moisture, and we also evaluated two types of TLS units: time of flight (TOF) and phase-shift (PS). A TOF lidar unit sends out a discrete pulse of energy and records the time it takes for the pulse to be reflected off a surface. Using the known speed of light, the object distance is calculated [64]. The advantage of TOF units is that multiple returns can be recorded for each pulse sent as a partial reflection of the energy is still recorded. The disadvantages are that surfaces in proximity to the scanner are often distorted and that each pulse must be returned before the next can be sent out. A PS lidar unit emits a continuous laser, and distance is calculated by using the phase shift of the incoming reflected energy relative to the phase of the outgoing energy. There are no discrete pulses of energy that are able to record multiple returns. PS tends to be faster with less distortion at close distances [65]. However, PS scanners tend to have a more limited range, mainly due to energy requirements. The different technologies exhibit slight differences in how intensity values are calculated [65–67].

1.4. Study Objectives

Lidar is becoming increasingly common with rapid advancements in field applications. In this study, we explored the ability of TLS to quantify fuel moisture in a controlled laboratory environment. The main objective was to demonstrate that a single TLS unit can provide a reliable measurement of fuel moisture in fuel beds comprising senesced leaf material, and to test whether TOF or PS lidar technology performed better. The intermediary objectives were to measure the relative change in fuel bed reflectance in relation to the water content with a passive sensor spectrometer to validate that the change in TLS intensity values correlated with a change in reflectance measured by the spectrometer. Another objective was to derive a host of potential metrics from the multiple intensity returns across a sample to determine which metric (or combination of metrics) had the strongest relationship to fuel moisture. The final objective was to determine if changing the angle of the fuel bed relative to the ground affected the relationship between the intensity

metrics and fuel moisture content of the samples. Additionally, a table of coefficients was developed for the relationships between the intensity metrics and moisture content for the different sample types and distances. A workflow diagram is presented in Figure 3 that outlines the study objectives and illustrates the structure of the study. If TLS scanning becomes an operational method for rapidly quantifying fuel moisture in potential fire fuels, it will be a valuable tool to aid in prescribed burning and fire behavior prediction. Intensity values were not calibrated to distance in this study to allow for a more direct comparison between the two scanners at set distances.

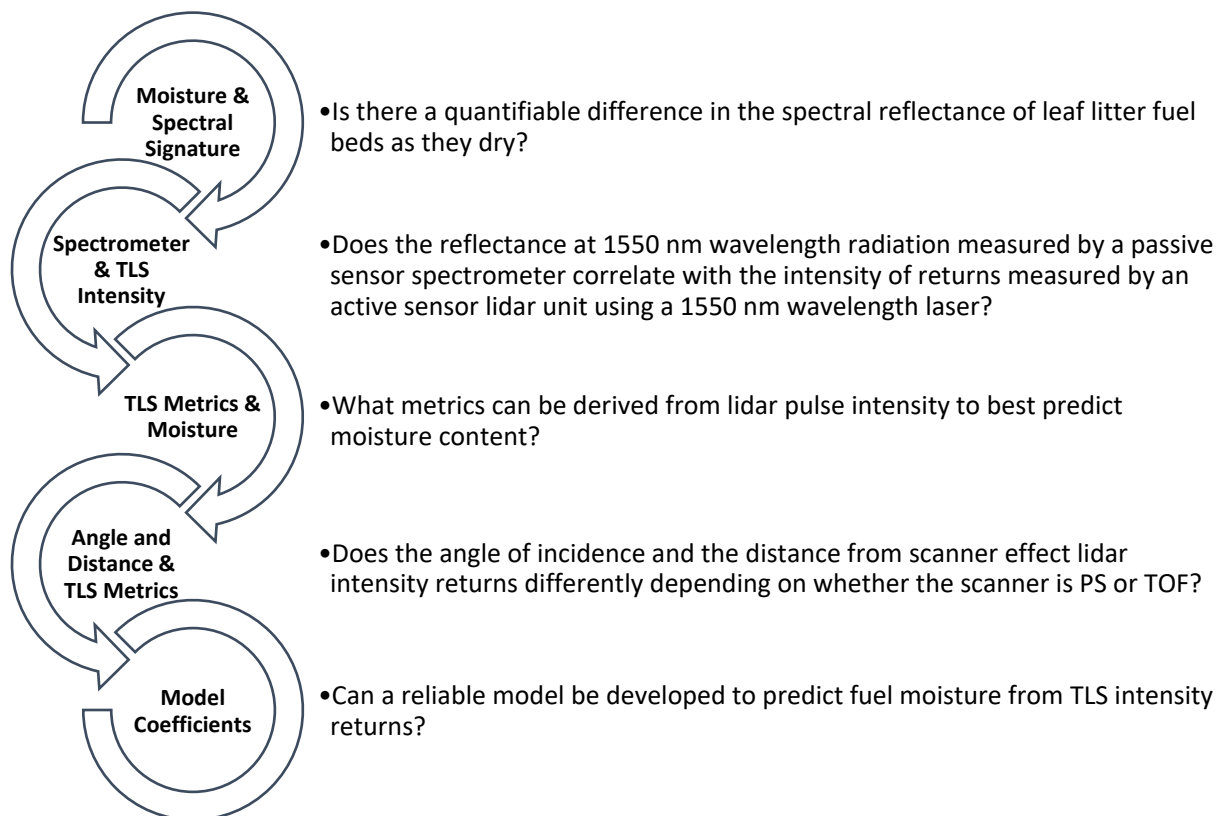


Figure 3. Workflow diagram of the research questions for this study and how they build upon each other to address the final goal of model development.

2. Materials and Methods

2.1. Materials

Six unique materials were used to evaluate the relationship between lidar reflectance and fuel moisture, including four common forest litter types and two controls (Table 1). Litter beds were constructed from senesced needle and broad leaf material collected from forest locations in Washington and northern Florida. The litter types included Douglas-fir (*Pseudotsuga menziesii*) needles, longleaf pine (*Pinus palustris*) needles, southern red oak (*Quercus falcata*) leaves, and ponderosa pine (*Pinus ponderosa*) needles. The litter samples were air-dried and sorted to remove any foreign particles. When assembling the leaf litter trays, care was taken to ensure that the litter completely occluded the tray to ensure all point returns were of the plant material and not the underlying tray. The sample trays were constructed of a non-porous white plastic material measuring 30 cm × 30 cm × 5 cm with a fine mesh screen as the base to allow for the draining of water. Sixteen samples (trays) of each litter type and control material were assembled.

Table 1. Sample types and weights used in this study. “Uncompacted” indicates the samples that naturally had a lot of open area with no readily defined depth. Litter fuels were allowed to extend upwards out of the sample trays to mimic natural conditions.

| Sample Type | Weight Range (Grams) | Weight Mean (Grams) | Depth of Sample |
|------------------------|----------------------|---------------------|-----------------|
| Douglas-fir (DF) | 119–156 | 135 | ~3 cm |
| Ponderosa pine (PP) | 104–158 | 129 | Uncompacted |
| Longleaf pine (LLP) | 70–123 | 101 | Uncompacted |
| Southern red oak (SRO) | 27–35 | 31 | Uncompacted |
| Fabric mesh (FM) | 66–74 | 67 | ~0.5 cm |
| Pine board (PB) | 514–596 | 569 | ~1.5 cm |

The two controls, milled pine wood and fabric mesh, were used to assess the influence of the scan angle on the intensity of the returns. The fabric mesh consisted of uniform layers of cotton cheese cloth (a gauze-like material) to mimic the porosity of forest litter. The other control material was milled, untreated pine board approximately 30 cm × 30 cm × 5 cm in size. Three of the sixteen Douglas-fir samples were removed from the analysis due to fine soil contamination that impacted the reflectance values.

2.2. Experimental Design

2.2.1. TLS Data Collection

The fuel moisture experiment was conducted at the Pacific Wildland Fire Sciences Laboratory in Seattle, WA. All the samples were fully saturated by soaking them in water for a minimum of 24 h in polyethylene bags. For scanning, the samples were arranged in sets of four and placed at a 3 m, 6 m, 9 m, and 12 m distance from the scanners (Figure 4). The samples were scanned simultaneously with PS and TOS units at 0 degrees (parallel to the ground) at each distance. The control surfaces were additionally scanned at 45 degrees and 90 degrees (perpendicular to the ground) (Table 2). The weight of each sample was recorded, and then the samples were rotated to the next defined distance and the process was repeated three times, so that each sample was scanned at all four scan locations.

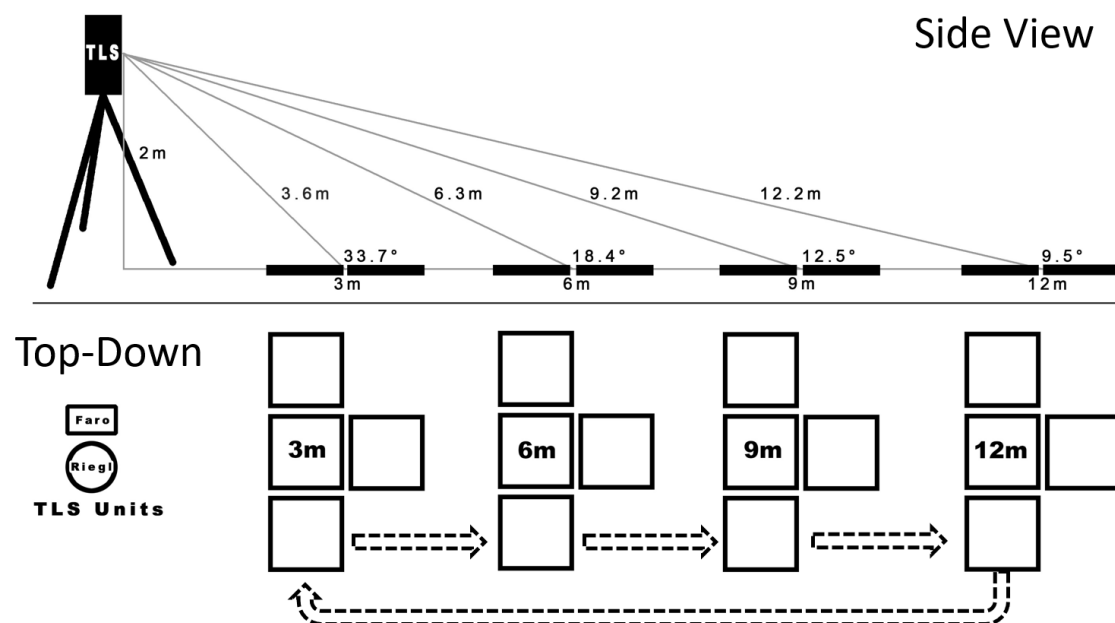


Figure 4. Layout of samples during scanning. Samples were moved in groups of 4. The arrow indicates the rotation direction used to scan every sample, at every location, at every time period. Sample orientation is referred to as 0 degrees which is perpendicular to the ground, but the angle to the scanner decreases as distance from scanner increases.

Table 2. Scanning intervals, starting with the time samples were removed from water bath (0). OD refers to oven-dry. N is the total number of sample trays clipped from all lidar point clouds and the number of weights recorded. Only the controls were scanned at angles other than 0.

| Sample Type | Scan Intervals (Hours from First Scan) | Angle | N * |
|------------------------|--|-----------|---------------------------|
| Pine board (PB) | 0, 2, 4, 8, 12, 24, 48, 72, 120, OD | 0, 45, 90 | 3840–lidar 1280–weight |
| Fabric mesh (FM) | 0, 2, 4, 8, 12, 24, 36, 48, OD | 0, 45, 90 | 3456–lidar 1152–weight |
| Douglas-fir (DF) | 0, 1, 2, 4, 8, 12, 24, 36, 48, OD | 0 | 1280 |
| Ponderosa pine (PP) | 0, 1, 2, 4, 8, 12, 24, 36, 48, 120, OD | 0 | 1408 |
| Longleaf pine (LLP) | 0, 1, 2, 4, 8, 12, 24, 36, 48, OD | 0 | 1280 |
| Southern red oak (SRO) | 0, 1, 2, 4, 8, 12, 24, 36, OD | 0 | 1152 |

* Number of samples = number of scans (4 distances) × number of trays (16) × scan intervals × 2 scanners (FARO & RIEGL) × 3 angles (PB & FM only).

After the initial scan (h 0), the process was repeated at the hourly time intervals of 1, 2, 4, 8, and 12 h since removal from the water bath, and then repeated every 12 h until the samples reached equilibrium moisture content with the ambient relative humidity (i.e., their weight stabilized and was no longer decreasing due to water evaporation). Scanning at four locations, weighing the samples, and rotating samples took approximately 50 min to one hour. Between scan times, the samples were placed in a climate-controlled room with ~25% relative humidity to allow for gradual drying. Drying times varied by material type (Table 2). Once the samples reached a stable weight, they were placed in a drying oven set at 70 °C until the samples reached a constant weight (48 h). A final set of scans was conducted immediately following the removal of the samples from the oven, and then the oven-dry weights were collected. Sample gravimetric moisture content was calculated by subtracting the final dry weight of the sample from the weight recorded during the drying process, then dividing it by the final oven-dried weight.

2.2.2. Spectrometer Data Collection

An ASD FieldSpec 4 Wide-Res field spectroradiometer [68] with a spectral resolution of 30 nm at 1400 to 2100 nm was used to collect the spectral information of each sample to compare this with the lidar-based reflectance values. The spectrometer lens was placed 33 cm above the tray at a perpendicular angle and an 8-degree lens was used to sample the approximate central 9 cm of each tray. The spectrometer was used when the samples were rotated through the 6 m distance location. The sample trays were individually taken into a dark room dedicated for the spectrometer using a tungsten bulb as a light source (approximate wavelength range of 320 nm to 2400 nm). A spectralon disk was used to calibrate the spectrometer before every measurement. The samples were checked to ensure that there were no gaps exposing the tray bottom. The white material of the tray sides likely reflected non-sample light back into the spectrometer sensor; this reflective phenomenon was the same for all trays, and thus it was constant. Moreover, for this study, we were only interested in the relative change in each sample as it dried, and not in gaining a true and precise measurement of the spectral signature of each sample material or equating an exact reflectance value as measured by the spectrometer to an exact intensity value from the TLS. Maintaining a consistent sampling environment and procedure, the relative change in spectral reflectance between the samples was measured.

2.3. Terrestrial Laser Scanners

Two 1550 nm wavelength TLS scanners including a time-of-flight RIEGL vz-2000 unit and phase-shift FARO s350 unit were used. A summary of the properties of each scanner is presented in Table 3. The scanning resolution settings of the FARO and RIEGL units were

chosen to provide a scanning time of approximately 3.5 min. The FARO unit scanned at a lower resolution than the RIEGL unit. A short scan time was prioritized over matching scanning resolutions to minimize the evaporation of water from the samples as they were rotated through the 4 scanning locations of each time interval. The number of points per sample decreased as the distance from the scanner increased in relation to the scan angle increment of each scanner (Table 3). The minimum number of points per sample tray was sampled 12 m from the FARO unit (~900 points), and the maximum number of points per sample tray was sampled 3 m from the RIEGL scanner (~103,000 points). The total area effectively sampled with each laser pulse also increased with distance as the laser footprint increased due to both the distance from the scanner as well as the angle of incidence. The TLS units were placed as closely as possible to each other (~20 cm) and were run simultaneously when scanning. This design was developed to balance the need to gather data rapidly (as the samples were actively losing moisture while TLS scanning was taking place) with the need to have sufficient replicants for statistical inference.

Table 3. Summaries of the two TLS units used for this study. Scan time was ~3.5 min with both scanners running simultaneously using 1550 nm wavelength laser light for each unit. Laser pulses intercepted the samples at differing angles for each distance. The footprint ellipsoid was significantly elongated at the further distances.

| Unit Specs | | | Approximate number of pulses per sample | | | |
|----------------|-----------------|------------------|---|-----------------------|-----------------------|------------------------|
| TLS | Min Range | Max Range | Scan Angle Increment | 3 m | 6 m | 9 m |
| FARO | 0.6 m | ~350 m | 0.018° | ~34,000 | ~6000 | ~2000 |
| RIEGL | 2.5 m | ~2000 m | 0.010° | ~103,000 | ~18,500 | ~6000 |
| Footprint Size | | | | | | |
| TLS | Beam Divergence | Diameter at Exit | Ellipsoid at 3 m (mm) | Ellipsoid at 6 m (mm) | Ellipsoid at 9 m (mm) | Ellipsoid at 12 m (mm) |
| FARO | 0.3 mrad * | 2.2 mm | 3.3 × 5.9 | 4.1 × 13 | 5 × 23.1 | 5.9 × 35.7 |
| RIEGL | 0.3 mrad | 18 mm | 19.1 × 34.4 | 19.9 × 63 | 20.8 × 96.1 | 21.7 × 131.5 |

* 0.3 mrad corresponds to an increase of 30 mm in beam diameter per 100 m of range.

2.4. Data Processing

The FARO software “Scene” [69] and the RIEGL software “Riscan Pro” [70] were used for the initial processing and conversion of the proprietary file formats into. LAS formats. To ensure that all valid returns from the sample trays were preserved, point cloud filtering was not conducted. This inclusive processing method included some amount of noise from edge effects and errant reflected laser light. However, it was deemed better to use all point returns to ensure all valid returns were included rather than try to filter out noise and subsequently remove valid point returns.

The RIEGL intensity values for the points ranged from 0 to 50 and the FARO intensity values ranged from 0 to 32,767 (scaled to a 15-bit radiometric resolution). After initial processing, the program CloudCompare [71] was used to manually crop out all points that were returns inside each sample tray. Care was taken to ensure that no points that were returns from the sample trays or tray bottoms were included in the clip based upon the intensity values of the points and their proximity to the edge or bottom. The RIEGL scanner has the ability to register multiple returns from each pulse emitted, but across all samples, only the first returns were within our clipping boundaries. Using only the first returns was not intentional but rather coincidental to how the data was processed. The intensity values were normalized between the FARO scans and the RIEGL scans by dividing each intensity value by the maximum value present in each scan. The normalization process scaled the intensity values between 0 to 1 for easier comparison between the two scanners. The intensity metrics derived per sample were the mean, median, 95th percentile, standard

deviation (SD), variance, and skew. Due to the confounding factors of the angle of incidence and surface texture, normalized intensity values were used in place of the intensity values and calibrated to represent surface reflectance.

2.5. Analysis

2.5.1. Spectrometer

An averaged spectral signature from the spectrometer sampling was created for each sample type at each sampling interval (i.e., the average value of each wavelength for all 16 ponderosa pine needle litter samples at the 2 h scan time interval). The reflectance values for each sample at 1550 nm were determined and compared with the moisture content recorded for all the samples at the 6 m distance. A simple ordinary least-squares (OLS) regression analysis was performed to determine if the reflectance measured by the spectrometer (response) had a significant relationship to moisture content (predictor). The reflectance values recorded by the spectrometer were also compared with the TLS intensity metrics recorded for all samples at the 6 m distance. A simple regression analysis was performed to determine if there was a significant relationship between the spectrometer-measured reflectance values and the recorded mean TLS intensity.

2.5.2. TLS Intensity

The regression models compared the intensity mean, median, 95th percentile, SD, variance, and skew of all the points within each sample. Three regression forms were evaluated, including a linear model, a first-order polynomial transformation, and a linear broken stick model, to determine what combination of the derived lidar intensity metrics performed best as predictor variables for the measured fuel moisture. Log and squared transformations were evaluated for the predictor variables, and a reduction in AIC (Akaike information criterion) values were used for the final selection of predictor variables. The AIC values were only calculated for model selection between the TLS variables and moisture content. There was a change in slope for the metrics at 100% moisture (an exception being pine board, for which a change in slope occurred at 40%); therefore, a broken stick regression approach was used. To conduct this, consider a breakpoint at $X = x_b$, and define:

$$I = \begin{cases} 0 & X < x_b \\ 1 & X \geq x_b \end{cases}$$

Then, the broken stick regression model can be written as:

$$Y = \beta_0 + \beta_1 X + \beta_2 I + \beta_3 X * I,$$

where β_0 and β_1 are the intercept and slope for $X < x_b$, and β_2 and β_3 are the change in intercept and slope moving from $X < x_b$ to $X \geq x_b$. Here, we applied the setting $x_b = 100$.

Finally, an analysis of covariance was performed to determine if the scan angle on the control samples significantly changed the coefficients between the lidar intensity and moisture content, treating the scan angle as a simple factor.

3. Results

3.1. Moisture & Spectral Signature

Sample moisture content ranged from 0% (oven dried weight) to 300% (fully saturated). The red oak leaves and the fabric mesh had the highest saturated moisture content and weighed three times the dried sample weight. The maximum moisture content for conifer needle litter ranged between 160% to 200%. The fully saturated pine boards reached approximately 65% moisture content.

The sample reflectance values at 1550 nm ranged from 0.1 when fully saturated to 0.6 when oven-dried (Figure 5). The highest variance between sample moisture content was generally observed at ~1450 nm, but a large spread of moisture values was also observed

around 1550 nm. The regression analysis showed that the sample reflectance at 1550 nm had a significant negative relationship ($p < 0.05$ for all sample materials) with the measured fuel moisture. The rate of the decrease, variance of the points, and shape of the relationship changed depending on the sample material. The coefficients of determination for the sample materials in regard to the reflectance measured at 1550 nm and the fuel moisture were as follows: Douglas-fir, 0.93; ponderosa pine, 0.9; longleaf pine, 0.84; southern red oak, 0.8; fabric mesh, 0.77; pine board, 0.84.

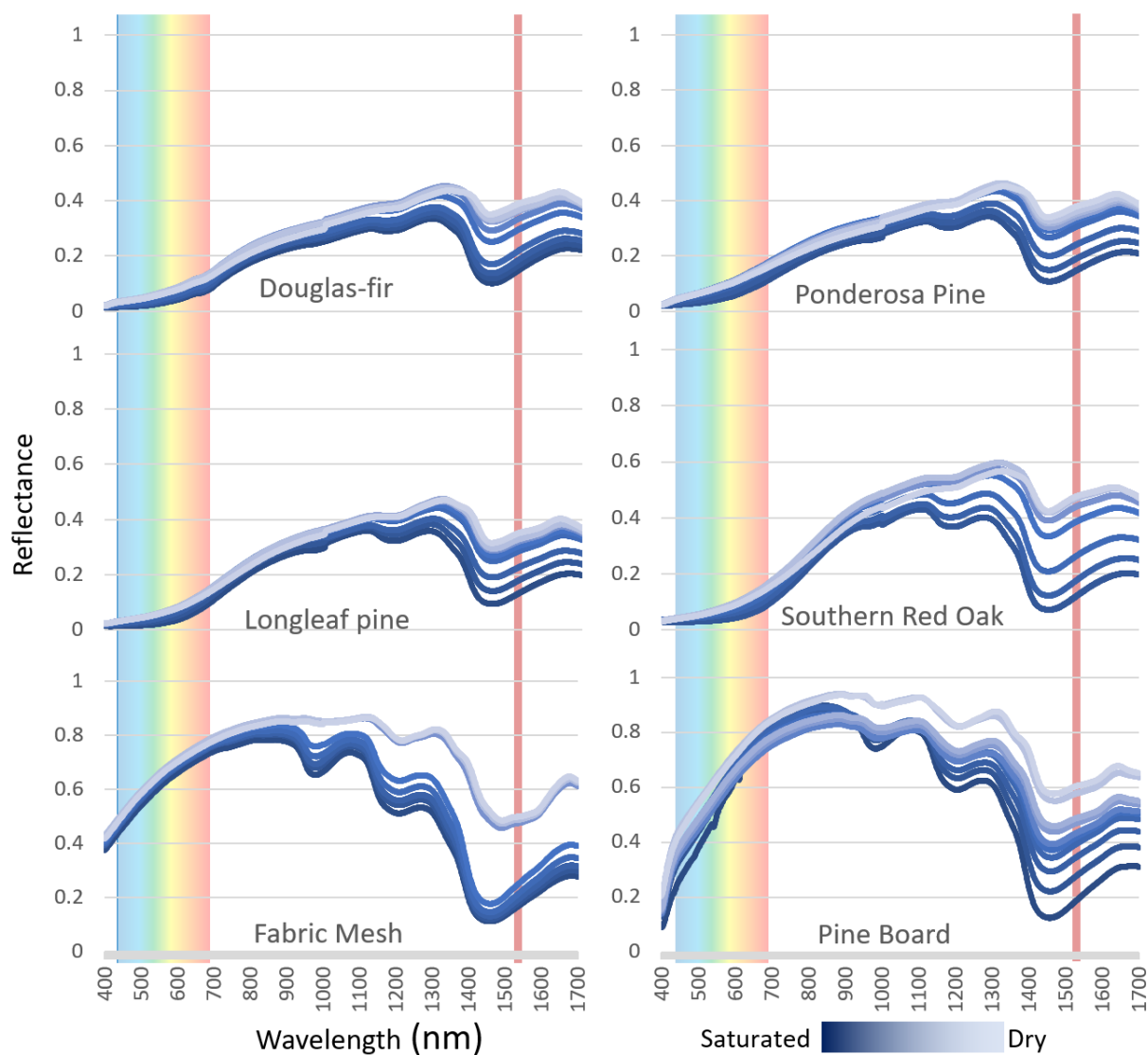


Figure 5. Average reflectance values by sample material and saturation level. The dark blue line represents samples at full saturation, with the color lightening to light blue for the final oven-dried reflectance values. The red line at 1550 nm represents the wavelength of the TLS units used for this experiment.

3.2. Spectrometer & TLS Intensity

The spectral reflectance at 1550 nm measured by the ASD spectrometer had a significant positive relationship ($p < 0.05$) with the normalized mean intensity values from the TLS units (Figure 6).

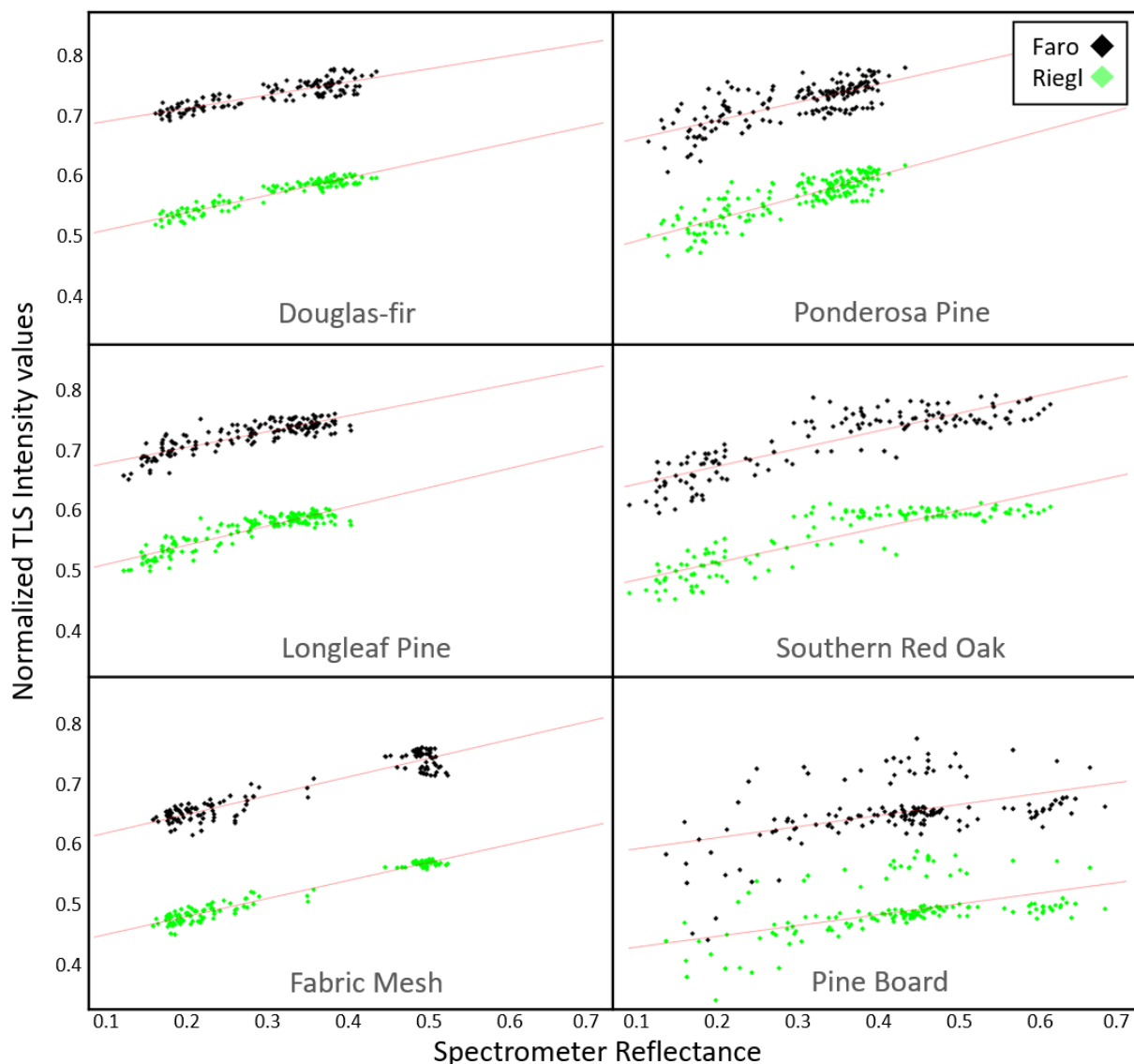


Figure 6. Linear relationship between reflectance values as measured by the spectrometer at 1550 nm and the mean intensity values of all lidar points from a sample. Intensity values were normalized on a scale between 0 and 1 for a direct comparison between the FARO and RIEGL units. The lower intensity values from the RIEGL unit are a product of this normalization and do not indicate that, overall, less energy was returned by each RIEGL pulse.

3.3. TLS Metrics & Moisture

Of the six lidar metrics (mean, median, 95th percentile, standard deviation (SD), variance, and skew), the mean, median, and 95th percentile were correlated ($>0.8 R^2$, $p < 0.05$). The standard deviation and variance were also correlated ($>0.8 R^2$, $p < 0.05$). However, there was no meaningful correlation between the mean and the standard deviation ($<0.25 R^2$, $p < 0.05$). The best-performing models with the highest coefficient of determination and lowest AIC value were the linear broken stick models using the mean intensity values with the break at 100% moisture content for all sample materials except the pine board. The pine board moisture content percentage never increased above 100% but the distinct change in slope occurred at 40% moisture content. The locations of the breaks were determined by where the slope of the linear relationship visually changed, with the exact subjective value of 100% being chosen as it was a value with an easily understood meaning (the weight of the sample was equal parts water and vegetation) and was uniformly a location across all material types (except the pine boards) where the slope of the relationship changed. The

mean of the lidar intensity values had the strongest correlation with the fuel moisture for the RIEGL data and performed well for the FARO data (Figure 7 and Supplemental Figure S1). However, the standard deviation of the intensity returns was also strongly correlated with the fuel moisture and was a better predictor for some FARO samples than mean intensity was (Figure 8). Images were produced using the point clouds from the FARO scanner to illustrate the change in the reflectance of the samples at 1550 nm (Supplemental Figure S2).

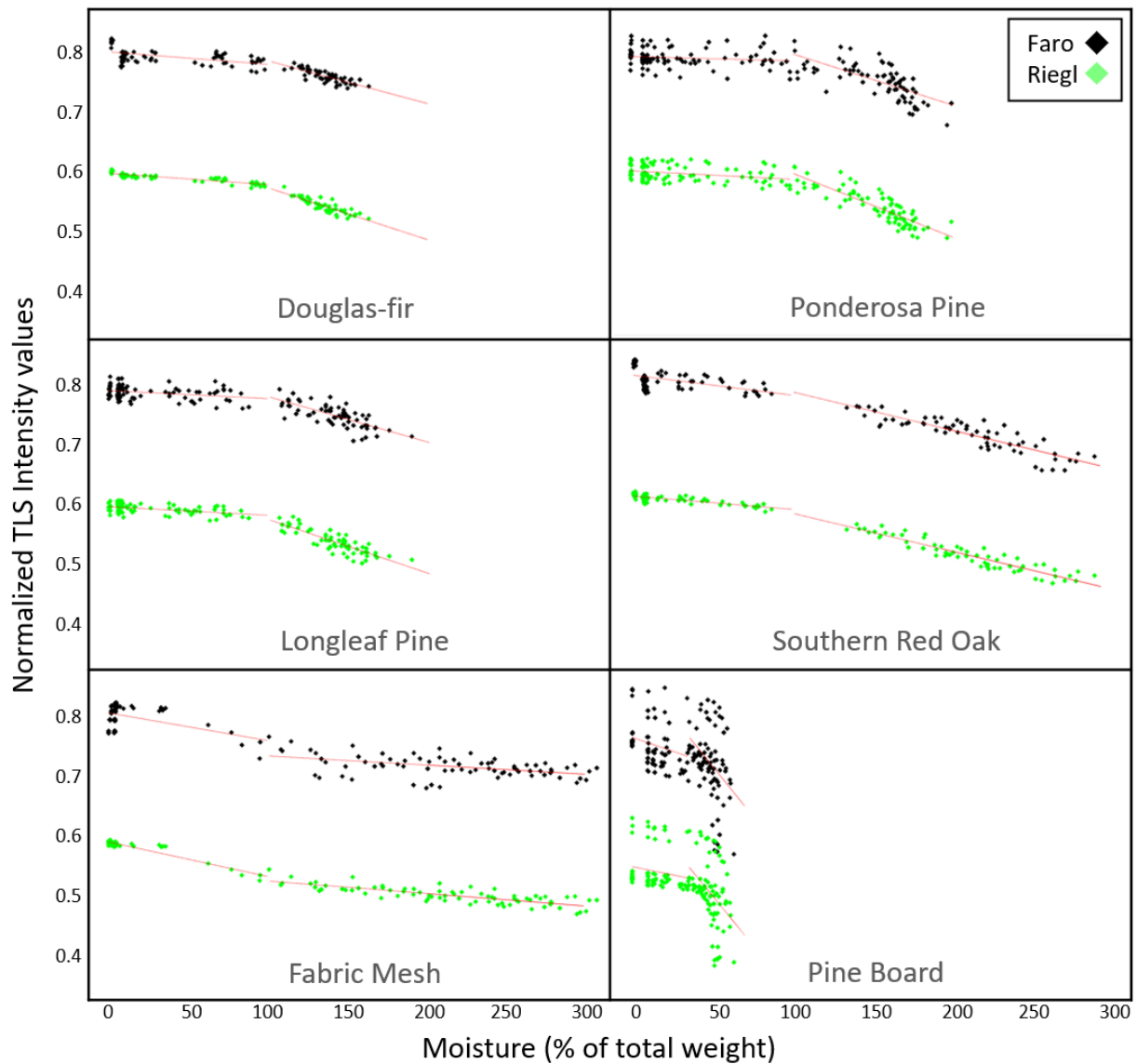


Figure 7. Mean normalized intensity values of the samples placed at 3 m from FARO and RIEGL scanners. Regression lines from a broken stick linear regression model are added. The selected break location was 100% for all sample materials except pine board for which the break was located at 40%.

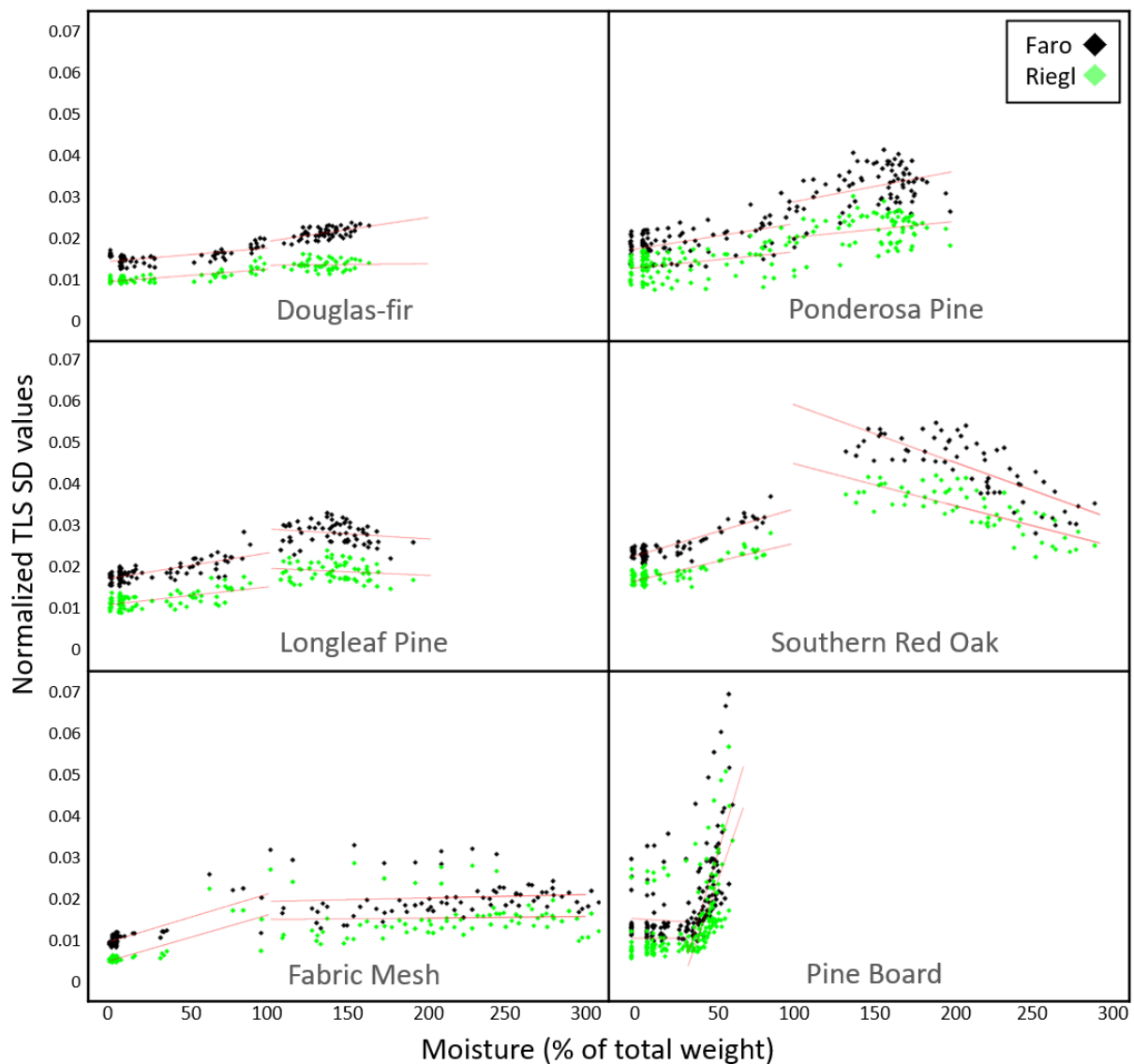


Figure 8. Standard deviation of normalized intensity values of the samples placed at 3 m from the FARO and RIEGL scanners. Regression lines from a broken stick linear regression model are added. The break location was 100% for all sample materials except pine board for which the break was located at 40%.

3.4. Angle and Distance & TLS Metrics

Correlations between reflectance and fuel moisture were comparable between the FARO and RIEGL units. However, beyond a distance of 3 m, the time-of-flight RIEGL unit performed much better than the FARO did at modeling fuel moisture. While the relationship deteriorated with distance for the RIEGL unit, the rate of deterioration was much lower than that of the FARO unit. Deterioration was related to the distance, the angle of incidence (Figure 4), and the footprint size (Table 2).

An ANCOVA test was performed to determine if the coefficients of the mean intensity values vs. the moisture content of the 45° and 90° control samples differed significantly from those of the 0° control samples. The normalized linear broken stick model coefficients are presented in the Supplemental Table S1, noting the coefficient values that were significantly different from the coefficient values of 0° samples. With the notable exception of the FARO data at 3 m, there was no significant difference between the coefficients for the 0° and 45° intensity values. In general, the coefficients did not significantly change until the samples were at an angle greater than 45°.

3.5. Model Coefficients

The coefficient of determination for the final broken stick models ranged from 0.98 for the southern red oak and fabric mesh samples at the 3 m distance to 0.07 for the long leaf pine at 12 m. With few exceptions, the regression models of the reflectance values from the TOF RIEGL unit had stronger model fits than those of the PS FARO unit, especially at the further distances (Table 4). A comprehensive table of the coefficients and R^2 values for the non-normalized data is included in Supplementary Table S2. Each sample type at each distance with moisture levels before and after the break in the regression line, using a multiple linear regression model for mean and SD reflectance, is shown below.

Table 4. Coefficient of determination values for multiple linear regression models across sample types. Mean intensity values of each sample and the standard deviation of each sample revealed the best fitting model. The figures 0, 45, and 90 indicate the sample angle relative to the ground. A more comprehensive table is presented in Supplementary Table S2.

| Mean & SD | | DF R^2 | PP R^2 | LLP R^2 | SRO R^2 | FM 0 R^2 | FM 45 R^2 | FM 90 R^2 | PB 0 R^2 | PB 45 R^2 | PB 90 R^2 |
|-----------|------|----------|----------|-----------|-----------|------------|-------------|-------------|------------|-------------|-------------|
| FARO | ALL | 0.65 | 0.40 | 0.28 | 0.83 | 0.66 | 0.84 | 0.88 | 0.25 | 0.44 | 0.49 |
| RIEGL | ALL | 0.86 | 0.56 | 0.69 | 0.95 | 0.92 | 0.94 | 0.92 | 0.32 | 0.54 | 0.50 |
| FARO | 3 M | 0.94 | 0.78 | 0.86 | 0.95 | 0.91 | 0.96 | 0.96 | 0.43 | 0.59 | 0.52 |
| RIEGL | 3 M | 0.95 | 0.76 | 0.90 | 0.98 | 0.96 | 0.98 | 0.98 | 0.46 | 0.65 | 0.61 |
| FARO | 6 M | 0.81 | 0.55 | 0.68 | 0.94 | 0.87 | 0.94 | 0.95 | 0.34 | 0.58 | 0.60 |
| RIEGL | 6 M | 0.92 | 0.60 | 0.79 | 0.97 | 0.94 | 0.97 | 0.98 | 0.38 | 0.58 | 0.63 |
| FARO | 9 M | 0.62 | 0.45 | 0.19 | 0.91 | 0.66 | 0.86 | 0.84 | 0.25 | 0.47 | 0.45 |
| RIEGL | 9 M | 0.83 | 0.51 | 0.72 | 0.96 | 0.93 | 0.97 | 0.97 | 0.30 | 0.55 | 0.67 |
| FARO | 12 M | 0.54 | 0.37 | 0.07 | 0.85 | 0.66 | 0.89 | 0.86 | 0.17 | 0.44 | 0.44 |
| RIEGL | 12 M | 0.88 | 0.49 | 0.68 | 0.93 | 0.92 | 0.97 | 0.97 | 0.26 | 0.50 | 0.67 |

4. Discussion

In this laboratory-based study, we quantified changes in fuel moisture using active sensor laser pulses at set distances from two 1550 nm lidar units. Beyond determining that lidar intensity returns can be used to estimate fuel moisture levels, we also determined that time-of-flight and phase-shift lidar units can both effectively measure changes in moisture in litter fuel beds. These findings corroborate those of studies that have used lidar to determine material characteristics using the intensity of return values [72,73]. They are also in line with those of numerous studies that have utilized dual-band TLS point clouds to determine live leaf moisture content [55,56,58]. However, this study provides an important new perspective on using a single wavelength TLS unit to determine the moisture content of wildland fuels. While we limited our study to common forest litter types, this study is an important step in utilizing active sensors to relate the spectral qualities of wildland fuels to fuel moisture while also capturing three-dimensional positional information.

4.1. Moisture & Spectral Signature

For this study, we first used standard spectrometry to confirm that there was a quantifiable difference in the spectral reflectance of leaf litter fuel beds as they air dried. The reflectance of all the samples increased as they dried. Increased reflectance with decreasing moisture content is well established [23,74,75], but quantifying the change in reflectance with a precise spectroradiometer allowed us to employ an established method to measure spectral reflectance changes instead of fully relying on a novel use of TLS to gauge change. We used the simple sampling technique of using a singular nadir view to measure the reflectance of the materials as they dried. The sampling angle, spectrometer footprint size, tray materials, and light source would all affect the values recorded by the spectrometer. The fact that reflectance changes as materials dry is well established. An exhaustive analysis of how spectrometer setup affects the reflectance values recorded was not the purpose of

this study. The use of the spectrometer was only for establishing if changes in moisture content detected by a well-established methodology using a spectrometer correlated with the changes in intensity recorded by a TLS unit.

4.2. Spectrometer & TLS Intensity

Reflectance at 1550 nm as recorded by the spectrometer was strongly correlated with the intensity values from the TLS units. Model fit differed among the sample types, with the lowest coefficient of determination being found for the pine boards. This was likely due to the heterogenous reflectance that was present, an artifact of the wood grain and knots. Aside from the pine boards, there was also a clear tendency for the more compact samples to have a higher coefficient of determination (e.g., Douglas-fir needles and the fabric mesh; Figure 6). The ponderosa pine, longleaf pine, and southern red oak were relatively uncompact, with there being large amounts of air space within the samples. The uncompact nature of these samples resulted in greater variability in their drying rates than in the drying rates of more compact samples. This structure also provided a more varied surface for the reflected lidar pulses compared to the more homogenous surface of a compact sample. Variances in the relationship between the spectrometer readings and the intensity returns from the TLS units were similar between the FARO and RIEGL units. It is important to note that we were only interested in the relative change in spectral reflectance as measured by the spectrometer and the intensity values of the TLS. Because the conditions in the spectrometer sampling and the lidar scanning were consistent, the relative difference with the change in the moisture content was successfully measured. The discernment of this relative difference is not to be confused with an attempt to determine the absolute conversion values between the spectrometer readings and TLS intensity values. For absolute values to be compared, such as when the x value from the spectrometer is equal to the x value from the TLS unit, a more rigorous sampling regimen would have been required, and potentially, confounding issues such as the angle of sampling would have needed to be accounted for. The view angle of the spectrometer was consistent at the nadir while the angle from the TLS scanner at 6 m was 18.4° (Figure 4). The spectrometer and the TLS scanner functionally saw different parts of the sample trays, but because we were only interested in if the relative change in reflectance measured by the spectrometer and the relative change in intensity measured by the TLS units were correlated, this difference in angle was not of concern.

4.3. TLS Metrics & Moisture

We evaluated a range of metrics that could be derived from the lidar pulse intensity. Of the seven metrics evaluated, the mean intensity per sample and the standard deviation of the intensity values per sample produced the most robust models. The broken stick linear regression models had high coefficients of determination, but relationships were strongest when the samples had a moisture content greater than 100%. At these moisture content levels, the strong relationship was likely only caused by surface water evaporation. This result suggests that lidar-based fuel moisture sensing will not be reliable in informing decisions based on fuel moisture content of less than 30%, which is typically required for prescribed burn planning [15,76]. However, lidar-based measurements could be helpful in remote stations that detect when live and dead fuel moistures are curing and potentially available for wildfires.

That intensity was related to dead fuel moisture levels in our study is consistent with other studies that have shown a relationship between lidar intensity and live leaf moisture content or building material moisture content. That we also found a relationship between the standard deviation of pulses per sample tray and fuel moisture is a more novel finding. It is observable that the surface of a sample becomes more homogeneous in its reflectance as it dries (Figure 2). With leaf litter, this is likely due to the fact that the litter will have varying levels of moisture content between the upper leaves that will dry faster relative to the lower leaves that will dry more slowly. This is more pronounced in the samples that

were less compacted, such as the long leaf pine. Additionally, the samples tended to be more compact when fully saturated, creating a more uniform surface with less variation in angles for the lidar pulses to reflect off.

4.4. Angle and Distance & TLS Metrics

We also evaluated if the angle of samples relative to the ground and distance of samples from scanner influenced the lidar intensity returns and how results differed between the PS and TOF sensors. While a strong relationship was found between laser pulse return intensity and fuel moisture, the relationship deteriorated with the distance from the scanner. This result was consistent between the PS and TOF scanners. The coefficients of the relationship between intensity and moisture also changed as the distance increased (Table 4, Figure S1). The TOF scanner maintained a stronger relationship as the distance increased while the PS scanner only had a strong relationship at close ranges. These findings are limited to a single study and are not sufficient for inferring that TOF units will always perform better than PS units for fuel moisture characterization. However, it is a significant finding that the type of lidar technology, the power of the laser, and potentially the size of the pulse footprint can affect the relationship. The footprint of the TOF RIEGL scanner is significantly larger than the footprint of the PS FARO scanner (Table 3). Subsequently, each lidar return from the RIEGL unit effectively samples a larger area. Because of the larger footprint size of the RIEGL unit, it is more likely for (especially at further distances) the returned intensity value to be a mixture of the reflectance from the materials inside the tray, the tray edge, and potentially the area outside the tray. This is likely minimized by the fact the RIEGL unit registers multiple returns per pulse, so the energy reflected from outside the tray should return to the RIEGL unit as a separate pulse return. It is unclear how much of an affect this had on the deteriorating strength of the relationship between the intensity and moisture as the distance increased.

For this study, we were interested in whether or not TLS can be used in the field, in which variability is inherent in the ground surface. As such, we were interested in the relative position of the samples to the ground and did not conduct an exhaustive analysis of the loss of the return intensity based on the true angle of incidence. The angle of incidence of each lidar pulse is determined not only by the orientation of the sample relative to the ground, but also by the distance of each sample from the scanner (Figure 4). When determining the regression lines for the samples at the tested angles, the Y intercept for all the 45° and 90° samples was greater than the intercept for the 0° samples (Figure S3), indicating that the former returned more energy than the 0° samples did. With a single exception being the fully saturated pine boards located 3 m from the FARO scanner, there was no significant difference between the regression coefficient for samples at 45° compared to samples at 0° relative to the ground. While numerous samples did demonstrate a significant difference between regression coefficients with samples at 90° compared to samples at 0°, these findings still present strong evidence that TLS intensity values maintain a consistent relationship to moisture content at least until the ground surface is at an angle of incidence greater than 45°. Further, it is important to consider that a significant difference in regression coefficients is determined not only by the linear trend of the data but also the spread of the data. Data clustered more tightly around the regression line will be more likely to show a significant difference between coefficients with a smaller change. Therefore, the RIEGL data, which tended to have a larger coefficient of determination than the FARO data, were more likely to show a significant difference in regression coefficients with a smaller change in the coefficient values. Past studies that have looked at the effect of the angle on intensity returns as they relate to moisture content have had mixed results [54,58,77]. That the angle influences the amount of energy returned is objectively true, but at what point that change degrades relationships between moisture content and intensity of return involves numerous additional variables, such as the specular nature of the reflecting surface. We speculate that the angle will have less of an effect on reflectance relationships with moisture content when the surface observed is a fuel bed on

the ground rather than individual leaves on a tree simply due to the spatial arrangement of surfaces being more uniform and less complex.

Intensity Calibration

Calibrating intensity values can have several different meanings. Interscan calibration can be conducted to ensure that the returned values are comparable between scans taken at different times in different conditions or that two different types of scanners are returning comparable values. We normalized the intensity values on a scale of 0 to 1 to facilitate the comparison between the scanners but this was not a true calibration for determining a transformation value by which the x value from the FARO scanner = x value from the RIEGL. The purpose of this study was not to derive coefficients to allow for the conversion of intensity values between two manufacturers of TLS units. Rather, we were interested in if the two scanners detected the relative change and one type of lidar technology outperformed the other in regard to its ability to quantify moisture content.

A calibration of intensity values can also be conducted to try and determine reflectance. This has been done in numerous studies utilizing TLS intensity values [43,55,63,78]. For our results to be applied in the field, a calibration of distance to model actual reflectance would need to be conducted to determine fuel moisture content at locations different from the distances sampled in this study.

4.5. Model Coefficients

The purpose of this study was to explore the relationships between different metrics derivable from TLS scans and the known fuel moisture levels of samples in a laboratory setting. Our initial results indicate that this methodology shows promise for future field applications in estimating the fuel moisture of forest litter from TLS intensity returns. Our results, with high levels of significance and high coefficients of determination, show that model development for field applications is possible. A variable model with the distance from the scanner incorporated will be necessary to provide reliable results. Further, most lidar datasets do not have calibrated intensity values, and the intensity values are generally relativized to a range of minimum and maximum intensity values returned within a scan. This inherently makes comparison between scans difficult. There are also numerous environmental factors that can influence lidar return values such as temperature and humidity [79,80]. We performed our experiment in a controlled laboratory environment in which we could be reasonably certain that no external factors would impact the intensity return values between the scans on different days.

4.6. Future Research

Given the limitations of using TLS intensity values listed above, the next step for the application of TLS and fuel moisture measurements is to take the scanners into the field for real-world data collection. This study provides the background and regression analysis parameters for applications in field-collected data. The goal is to operationalize lidar scanning to quantify fuel moisture levels beyond the use of TLS for fine scale moisture mapping from a stationary location. More research needs to be conducted to potentially calibrate intensity values to distance. Beyond simple distance calibration, it should also be investigated if the relationship between standard deviation and moisture is affected by distance. Further, we used “pure” fuel samples of leaves from a single species. More work is needed to determine if a generalized model can be produced that can be applied to mixed fuel beds found in field settings. If a reliable calibration to convert intensity to reflectance can be conducted, then this process has potential for mapping larger areas using drones and mobile lidar units. A drone-based lidar unit sampling at a 1550 nm wavelength could cover a much larger area with a more consistent distance from the ground than a stationary tripod mounted TLS could.

Applications beyond fuel moisture mapping are numerous. A drone-based lidar unit could also be used for the detection and verification of wetland below the canopy by

isolating only the ground returns and determining the locations of inundated soils and vegetation. While ALS has been used to detect inundated areas under the canopy [39], a drone-based approach would allow for the intentional selection of a lidar sensor using a 1550 nm wavelength as well as greater temporal resolution of resampling. Any investigation in which the detection of ground moisture is important could take advantage of the benefits of using an active sensor over a passive sensor spectroradiometer.

5. Conclusions

Fuel moisture is a critical variable for wildland fire management but is costly and inefficient to sample with traditional methods. Drone-based techniques using spectral reflectance values are being developed [25,81] to estimate moisture levels at a fine spatial scale, but the use of active sensors such as lidar sensors can present advantages over the use of passive sensors. Specifically, lidar sensors can penetrate through small gaps in forest cover to derive measurements for fine-scale terrain mapping. This characteristic makes it possible to derive information about ground moisture content via the intensity values of surfaces that are not detectable by passive sensors. As further studies evaluate the application of lidar sensors in moisture sampling, this developing research field will be of great interest to designated fire managers and scientists working on fire behavior prediction and fire ecology.

Because of the weaker relationships that exist with lower fuel moisture values, there may be limitations to the use of TLS to inform decisions about wildland fire behavior, but it can be useful to determine moisture gradients and seasonal shifts in fuel availability for combustion, and to detect areas with high moisture and water content such as seeps and small wetlands. These are preliminary findings that indicate that active sensors such as lidar sensors provide the potential ability to quantify moisture content based on the intensity and variation of intensity values. To further evaluate this method, field studies need to be conducted to measure TLS measurements coupled with field measurements of litter moisture to verify the ability of TLS to quantify fuel moisture outside of a laboratory environment. This study sets the groundwork for the future use of lidar as a moisture detection tool that will allow for the rapid, onsite, and continuous quantification of forest litter moisture content.

Supplementary Materials: The following supporting information can be downloaded at: <https://www.mdpi.com/article/10.3390/rs15061482/s1>, Figure S1: Mean intensity values of all samples across all distances; Figure S2: Images produced from the FARO laser scanner of a representative of each sample type fully saturated; Figure S3: Scatter plot of all control samples at the three different angles; Table S1: Coefficient values; Table S2: Comprehensive table of the coefficients and R^2 values.

Author Contributions: Conceptualization, J.L.B., E.R. and S.P.; methodology, J.L.B., E.R., S.P., D.N. and L.M.M.; software, J.L.B.; validation, E.R., S.P., D.N. and M.C.K.; formal analysis, J.L.B. and M.C.K.; investigation, J.L.B., D.N. and J.C.; resources, E.R., S.P. and L.M.M.; data curation, J.L.B., D.N. and J.C.; writing—original draft preparation, J.L.B.; writing—review and editing, E.R., S.P., D.N., J.C., M.C.K. and L.M.M.; visualization, J.L.B.; supervision, S.P. and L.M.M.; project administration, S.P. and L.M.M.; funding acquisition, S.P. and L.M.M. All authors have read and agreed to the published version of the manuscript.

Funding: U.S. Department of Defense Strategic Environmental Research and Development Program Project # RC-19-C1-1064. Precision Forestry Cooperative, University of Washington for research funding and instrumentation.

Institutional Review Board Statement: Not applicable.

Informed Consent Statement: Not applicable.

Data Availability Statement: Data available on request.

Acknowledgments: We want to thank members of the Fire and Environmental Applications Team field crew, including Jessie C Thoreson and Nick Tripodi, for help with the laboratory experiments. We also thank Brian Drye for help with data processing and analysis.

Conflicts of Interest: The authors declare no conflict of interest.

References

1. Rothermel, R.C. *A Mathematical Model for Predicting Fire Spread in Wildland Fuels*; Intermountain Forest & Range Experiment Station, Forest Service, US Department of Agriculture: Ogden, UT, USA, 1972; Volume 115.
2. Rothermel, R.C. *How to Predict the Spread and Intensity of Forest and Range Fires*; US Department of Agriculture, Forest Service, Intermountain Forest and Range: Ogden, UT, USA, 1983; Volume 143.
3. Countryman, C.M. Moisture in Living Fuels Affects Fire Behavior. *Fire Manag.* **1974**, *35*, 10–14.
4. Jolly, W.M. Sensitivity of a Surface Fire Spread Model and Associated Fire Behaviour Fuel Models to Changes in Live Fuel Moisture. *Int. J. Wildland Fire* **2007**, *16*, 503–509. [[CrossRef](#)]
5. Matthews, S. Dead Fuel Moisture Research: 1991–2012. *Int. J. Wildland Fire* **2014**, *23*, 78–92. [[CrossRef](#)]
6. Flannigan, M.D.; Wotton, B.M.; Marshall, G.A.; De Groot, W.J.; Johnston, J.; Jurko, N.; Cantin, A.S. Fuel Moisture Sensitivity to Temperature and Precipitation: Climate Change Implications. *Clim. Chang.* **2016**, *134*, 59–71. [[CrossRef](#)]
7. Viney, N.R. A Review of Fine Fuel Moisture Modelling. *Int. J. Wildland Fire* **1991**, *1*, 215–234. [[CrossRef](#)]
8. Keane, R.E.; Gray, K. Comparing Three Sampling Techniques for Estimating Fine Woody down Dead Biomass. *Int. J. Wildland Fire* **2013**, *22*, 1093–1107. [[CrossRef](#)]
9. Rowell, E.; Prichard, S.; Varner, J.M.; Shearman, T.M. Re-Envisioning Fire and Vegetation Feedbacks. In *Wildland Fire Dynamics*; Speer, K., Goodrick, S., Eds.; Cambridge University Press: Cambridge, UK, 2022; pp. 156–182, ISBN 978-1-108-58024-3.
10. Yebra, M.; Dennison, P.E.; Chuvieco, E.; Riaño, D.; Zylstra, P.; Hunt, E.R.; Danson, F.M.; Qi, Y.; Jurdao, S. A Global Review of Remote Sensing of Live Fuel Moisture Content for Fire Danger Assessment: Moving towards Operational Products. *Remote Sens. Environ.* **2013**, *136*, 455–468. [[CrossRef](#)]
11. Pimont, F.; Parsons, R.; Rigolot, E.; de Coligny, F.; Dupuy, J.-L.; Dreyfus, P.; Linn, R.R. Modeling Fuels and Fire Effects in 3D: Model Description and Applications. *Environ. Model. Softw.* **2016**, *80*, 225–244. [[CrossRef](#)]
12. Gergel, D.R.; Nijssen, B.; Abatzoglou, J.T.; Lettenmaier, D.P.; Stumbaugh, M.R. Effects of Climate Change on Snowpack and Fire Potential in the Western USA. *Clim. Chang.* **2017**, *141*, 287–299. [[CrossRef](#)]
13. Ma, W.; Zhai, L.; Pivovarov, A.; Shuman, J.; Buotte, P.; Ding, J.; Christoffersen, B.; Knox, R.; Moritz, M.; Fisher, R. Assessing Climate Change Impacts on Live Fuel Moisture and Wildfire Risk Using a Hydrodynamic Vegetation Model. *Biogeosciences* **2021**, *18*, 4005–4020. [[CrossRef](#)]
14. Rossa, C.G.; Fernandes, P.M. Live Fuel Moisture Content: The ‘Pea under the Mattress’ of Fire Spread Rate Modeling? *Fire* **2018**, *1*, 43. [[CrossRef](#)]
15. Pollet, J.; Brown, A. *Fuel Moisture Sampling Guide*; Utah State Office, Bureau of Land Management: Salt Lake City, UT, USA, 2007.
16. Haines, D.A.; Frost, J.S. *Weathering Effects on Fuel Moisture Sticks: Corrections and Recommendations*; Department of Agriculture, Forest Service, North Central Forest Experiment: St. Paul, MN, USA, 1978; Volume 154.
17. Ceccato, P.; Gobron, N.; Flasse, S.; Pinty, B.; Tarantola, S. Designing a Spectral Index to Estimate Vegetation Water Content from Remote Sensing Data: Part 1: Theoretical Approach. *Remote Sens. Environ.* **2002**, *82*, 188–197. [[CrossRef](#)]
18. Datt, B. Remote Sensing of Water Content in Eucalyptus Leaves. *Aust. J. Bot.* **1999**, *47*, 909–923. [[CrossRef](#)]
19. Tian, Q.; Tong, Q.; Pu, R.; Guo, X.; Zhao, C. Spectroscopic Determination of Wheat Water Status Using 1650–1850 Nm Spectral Absorption Features. *Int. J. Remote Sens.* **2001**, *22*, 2329–2338. [[CrossRef](#)]
20. Tucker, C.J. Remote Sensing of Leaf Water Content in the near Infrared. *Remote Sens. Environ.* **1980**, *10*, 23–32. [[CrossRef](#)]
21. Wang, J.; Xu, R.; Yang, S. Estimation of Plant Water Content by Spectral Absorption Features Centered at 1450 Nm and 1940 Nm Regions. *Environ. Monit. Assess.* **2008**, *157*, 459. [[CrossRef](#)]
22. Makowiecki, A.S.; Steinbrenner, J.E.; Wimer, N.T.; Glusman, J.F.; Lapointe, C.B.; Daily, J.W.; Hamlington, P.E.; Rieker, G.B. Dual Frequency Comb Spectroscopy of Solid Fuel Pyrolysis and Combustion: Quantifying the Influence of Moisture Content in Douglas Fir. *Fire Saf. J.* **2020**, *116*, 103185. [[CrossRef](#)]
23. Qi, Y.; Dennison, P.E.; Jolly, W.M.; Kropp, R.C.; Brewer, S.C. Spectroscopic Analysis of Seasonal Changes in Live Fuel Moisture Content and Leaf Dry Mass. *Remote Sens. Environ.* **2014**, *150*, 198–206. [[CrossRef](#)]
24. Watanabe, K.; Mansfield, S.D.; Avramidis, S. Application of Near-Infrared Spectroscopy for Moisture-Based Sorting of Green Hem-Fir Timber. *J. Wood Sci.* **2011**, *57*, 288–294. [[CrossRef](#)]
25. Barber, N.; Alvarado, E.; Kane, V.R.; Mell, W.E.; Moskal, L.M. Estimating Fuel Moisture in Grasslands Using UAV-Mounted Infrared and Visible Light Sensors. *Sensors* **2021**, *21*, 6350. [[CrossRef](#)] [[PubMed](#)]
26. Vinnikov, K.Y.; Robock, A.; Qiu, S.; Entin, J.K.; Owe, M.; Choudhury, B.J.; Hollinger, S.E.; Njoku, E.G. Satellite Remote Sensing of Soil Moisture in Illinois, United States. *J. Geophys. Res. Atmos.* **1999**, *104*, 4145–4168. [[CrossRef](#)]
27. Wang, L.; Qu, J.J. Satellite Remote Sensing Applications for Surface Soil Moisture Monitoring: A Review. *Front. Earth Sci. China* **2009**, *3*, 237–247. [[CrossRef](#)]
28. Dragozi, E.; Giannaros, T.M.; Kotroni, V.; Lagouvardos, K.; Koletsis, I. Dead Fuel Moisture Content (DFMC) Estimation Using MODIS and Meteorological Data: The Case of Greece. *Remote Sens.* **2021**, *13*, 4224. [[CrossRef](#)]
29. Hao, X.; Qu, J.J. Retrieval of Real-Time Live Fuel Moisture Content Using MODIS Measurements. *Remote Sens. Environ.* **2007**, *108*, 130–137. [[CrossRef](#)]

30. Gillon, D.; Dauriac, F.; Deshayes, M.; Valette, J.C.; Moro, C. Estimation of Foliage Moisture Content Using near Infrared Reflectance Spectroscopy. *Agric. For. Meteorol.* **2004**, *124*, 51–62. [[CrossRef](#)]
31. Kemppinen, J.; Niittynen, P.; Riihimäki, H.; Luoto, M. Modelling Soil Moisture in a High-Latitude Landscape Using LiDAR and Soil Data. *Earth Surf. Process. Landf.* **2018**, *43*, 1019–1031. [[CrossRef](#)]
32. Carson, W.W.; Andersen, H.-E.; Reutebuch, S.E.; McGaughey, R.J. LIDAR Applications in Forestry—An Overview. In Proceedings of the ASPRS Annual Conference, Denver, CO, USA, 23–28 May 2004; pp. 1–9.
33. Dubayah, R.O.; Drake, J.B. Lidar Remote Sensing for Forestry. *J. For.* **2000**, *98*, 44–46.
34. Hudak, A.T.; Evans, J.S.; Stuart Smith, A.M. LiDAR Utility for Natural Resource Managers. *Remote Sens.* **2009**, *1*, 934–951. [[CrossRef](#)]
35. Wulder, M.A.; White, J.C.; Nelson, R.F.; Næsset, E.; Ørka, H.O.; Coops, N.C.; Hilker, T.; Bater, C.W.; Gobakken, T. Lidar Sampling for Large-Area Forest Characterization: A Review. *Remote Sens. Environ.* **2012**, *121*, 196–209. [[CrossRef](#)]
36. Stavros, E.N.; Coen, J.; Peterson, B.; Singh, H.; Kennedy, K.; Ramirez, C.; Schimel, D. Use of Imaging Spectroscopy and LIDAR to Characterize Fuels for Fire Behavior Prediction. *Remote Sens. Appl. Soc. Environ.* **2018**, *11*, 41–50. [[CrossRef](#)]
37. Bright, B.C.; Hudak, A.T.; McGaughey, R.; Andersen, H.-E.; Negrón, J. Predicting Live and Dead Tree Basal Area of Bark Beetle Affected Forests from Discrete-Return Lidar. *Can. J. Remote Sens.* **2013**, *39*, S99–S111. [[CrossRef](#)]
38. Korpela, I.; Ørka, H.O.; Hyyppä, J.; Heikkinen, V.; Tokola, T. Range and AGC Normalization in Airborne Discrete-Return LiDAR Intensity Data for Forest Canopies. *ISPRS J. Photogramm. Remote Sens.* **2010**, *65*, 369–379. [[CrossRef](#)]
39. Lang, M.W.; Kim, V.; McCarty, G.W.; Li, X.; Yeo, I.-Y.; Huang, C.; Du, L. Improved Detection of Inundation below the Forest Canopy Using Normalized LiDAR Intensity Data. *Remote Sens.* **2020**, *12*, 707. [[CrossRef](#)]
40. Garroway, K.; Hopkinson, C.; Jamieson, R. Surface Moisture and Vegetation Influences on Lidar Intensity Data in an Agricultural Watershed. *Can. J. Remote Sens.* **2011**, *37*, 275–284. [[CrossRef](#)]
41. Krooks, A.; Kaasalainen, S.; Hakala, T.; Nevalainen, O. Correction of Intensity Incidence Angle Effect in Terrestrial Laser Scanning. *ISPRS Ann. Photogramm. Remote Sens. Spat. Inf. Sci.* **2013**, *2*, 145–150. [[CrossRef](#)]
42. Hasegawa, H. Evaluations of LIDAR Reflectance Amplitude Sensitivity towards Land Cover Conditions. *Bull. Geogr. Surv. Inst.* **2006**, *53*, 43–50.
43. Kashani, A.G.; Olsen, M.J.; Parrish, C.E.; Wilson, N. A Review of LiDAR Radiometric Processing: From Ad Hoc Intensity Correction to Rigorous Radiometric Calibration. *Sensors* **2015**, *15*, 28099–28128. [[CrossRef](#)]
44. Loudermilk, E.L.; Hiers, J.K.; O'Brien, J.J.; Mitchell, R.J.; Singhanian, A.; Fernandez, J.C.; Cropper, W.P.; Slatton, K.C. Ground-Based LIDAR: A Novel Approach to Quantify Fine-Scale Fuelbed Characteristics. *Int. J. Wildland Fire* **2009**, *18*, 676–685. [[CrossRef](#)]
45. Rowell, E.; Seielstad, C. Characterizing Grass, Litter, and Shrub Fuels in Longleaf Pine Forest Pre-and Post-Fire Using Terrestrial LiDAR. In Proceedings of the SilviLaser, Vancouver, BC, Canada, 16–19 September 2012; pp. 16–19.
46. Rowell, E.M.; Seielstad, C.A.; Ottmar, R.D. Development and Validation of Fuel Height Models for Terrestrial Lidar-RxCADRE 2012. *Int. J. Wildland Fire* **2015**, *25*, 38–47. [[CrossRef](#)]
47. Plyler, E.K.; Sleator, W.W. Further Study of the Absorption of Infrared Radiation by Water Vapor. *Phys. Rev.* **1931**, *37*, 1493. [[CrossRef](#)]
48. Ponomarev, O.A.; Zakir'ianov, F.K.; Terpugov, E.L.; Fesenko, E.E. Absorption of Infrared Radiation by a Thin Water Layer. *Biofizika* **2001**, *46*, 402–407.
49. Suchocki, C.; Katzer, J.; Rapiński, J. Terrestrial Laser Scanner as a Tool for Assessment of Saturation and Moisture Movement in Building Materials. *Period. Polytech. Civ. Eng.* **2018**, *62*, 694–699. [[CrossRef](#)]
50. Suchocki, C.; Katzer, J. Terrestrial Laser Scanning Harnessed for Moisture Detection in Building Materials—Problems and Limitations. *Autom. Constr.* **2018**, *94*, 127–134. [[CrossRef](#)]
51. Jin, J.; De Sloover, L.; Verbeurgt, J.; Stal, C.; Deruyter, G.; Montreuil, A.-L.; De Maeyer, P.; De Wulf, A. Measuring Surface Moisture on a Sandy Beach Based on Corrected Intensity Data of a Mobile Terrestrial LiDAR. *Remote Sens.* **2020**, *12*, 209. [[CrossRef](#)]
52. Danson, F.M.; Gaulton, R.; Armitage, R.P.; Disney, M.; Gunawan, O.; Lewis, P.; Pearson, G.; Ramirez, A.F. Developing a Dual-Wavelength Full-Waveform Terrestrial Laser Scanner to Characterize Forest Canopy Structure. *Agric. For. Meteorol.* **2014**, *198*, 7–14. [[CrossRef](#)]
53. Gaulton, R.; Danson, F.M.; Pearson, G.; Lewis, P.E.; Disney, M. The Salford Advanced Laser Canopy Analyser (SALCA): A Multispectral Full Waveform LiDAR for Improved Vegetation Characterisation. In Proceedings of the Remote Sensing and Photogrammetry Society Conference, Remote Sensing and the Carbon Cycle, London, UK, 5 May 2010; Volume 5.
54. Hancock, S.; Gaulton, R.; Danson, F.M. Angular Reflectance of Leaves with a Dual-Wavelength Terrestrial Lidar and Its Implications for Leaf-Bark Separation and Leaf Moisture Estimation. *IEEE Trans. Geosci. Remote Sens.* **2017**, *55*, 3084–3090. [[CrossRef](#)]
55. Elsherif, A.; Gaulton, R.; Mills, J. Estimation of Vegetation Water Content at Leaf and Canopy Level Using Dual-Wavelength Commercial Terrestrial Laser Scanners. *Interface Focus* **2018**, *8*, 20170041. [[CrossRef](#)] [[PubMed](#)]
56. Gaulton, R.; Danson, F.M.; Ramirez, F.A.; Gunawan, O. The Potential of Dual-Wavelength Laser Scanning for Estimating Vegetation Moisture Content. *Remote Sens. Environ.* **2013**, *132*, 32–39. [[CrossRef](#)]
57. Junttila, S.; Sugano, J.; Vastaranta, M.; Linnakoski, R.; Kaartinen, H.; Kukko, A.; Holopainen, M.; Hyyppä, H.; Hyyppä, J. Can Leaf Water Content Be Estimated Using Multispectral Terrestrial Laser Scanning? A Case Study with Norway Spruce Seedlings. *Front. Plant Sci.* **2018**, *9*, 299. [[CrossRef](#)] [[PubMed](#)]

58. Junttila, S.; Vastaranta, M.; Liang, X.; Kaartinen, H.; Kukko, A.; Kaasalainen, S.; Holopainen, M.; Hyyppä, H.; Hyyppä, J. Measuring Leaf Water Content with Dual-Wavelength Intensity Data from Terrestrial Laser Scanners. *Remote Sens.* **2017**, *9*, 8. [[CrossRef](#)]
59. Junttila, S.; Hölttä, T.; Puttonen, E.; Katoh, M.; Vastaranta, M.; Kaartinen, H.; Holopainen, M.; Hyyppä, H. Terrestrial Laser Scanning Intensity Captures Diurnal Variation in Leaf Water Potential. *Remote Sens. Environ.* **2021**, *255*, 112274. [[CrossRef](#)]
60. Elsherif, A.; Gaulton, R.; Shenkin, A.; Malhi, Y.; Mills, J. Three Dimensional Mapping of Forest Canopy Equivalent Water Thickness Using Dual-Wavelength Terrestrial Laser Scanning. *Agric. For. Meteorol.* **2019**, *276*, 107627. [[CrossRef](#)]
61. Elsherif, A.; Gaulton, R.; Mills, J.P. The Potential of Dual-Wavelength Terrestrial Laser Scanning in 3d Canopy Fuel Moisture Content Mapping. *ISPRS Geospat. Week* **2019**, *XLII-2/W13*, 975–979. [[CrossRef](#)]
62. Calders, K.; Disney, M.I.; Armston, J.; Burt, A.; Brede, B.; Origo, N.; Muir, J.; Nightingale, J. Evaluation of the Range Accuracy and the Radiometric Calibration of Multiple Terrestrial Laser Scanning Instruments for Data Interoperability. *IEEE Trans. Geosci. Remote Sens.* **2017**, *55*, 2716–2724. [[CrossRef](#)]
63. Tan, K.; Chen, J.; Qian, W.; Zhang, W.; Shen, F.; Cheng, X. Intensity Data Correction for Long-Range Terrestrial Laser Scanners: A Case Study of Target Differentiation in an Intertidal Zone. *Remote Sens.* **2019**, *11*, 331. [[CrossRef](#)]
64. Raj, T.; Hashim, F.H.; Huddin, A.B.; Ibrahim, M.F.; Hussain, A. A Survey on LiDAR Scanning Mechanisms. *Electronics* **2020**, *9*, 741. [[CrossRef](#)]
65. Suchocki, C. Comparison of Time-of-Flight and Phase-Shift TLS Intensity Data for the Diagnostics Measurements of Buildings. *Materials* **2020**, *13*, 353. [[CrossRef](#)]
66. Calders, K.; Adams, J.; Armston, J.; Bartholomeus, H.; Bauwens, S.; Bentley, L.P.; Chave, J.; Danson, F.M.; Demol, M.; Disney, M.; et al. Terrestrial Laser Scanning in Forest Ecology: Expanding the Horizon. *Remote Sens. Environ.* **2020**, *251*, 112102. [[CrossRef](#)]
67. San José Alonso, J.I.; Martínez Rubio, J.; Fernández Martín, J.J.; García Fernández, J. Comparing Time-Of and Phase-Shift the Survey of the Royal Pantheon in the Basilica of San Isidoro (LEÓN). *ISPRS—Int. Arch. Photogramm. Remote Sens. Spat. Inf. Sci.* **2011**, *3816*, 377–385. [[CrossRef](#)]
68. ASD ASD FieldSpec 4 Wide-Res Field Spectroradiometer. Available online: <https://www.Malvernpanalytical.Com/2017> (accessed on 11 December 2021).
69. FARO Scene [Computer Software]; Version 2019.2. Available online: <http://www.faro.com> (accessed on 1 March 2021).
70. Riegl RiScan Pro [Computer Software]; Version 2.6.1; 2021. Available online: <https://www.riegl.com/> (accessed on 1 March 2021).
71. CloudCompare [Computer Software]; Version 2.11; 2019. Available online: <http://www.cloudcompare.org> (accessed on 1 March 2021).
72. Di Biase, V.; Hanssen, R.F.; Vos, S.E. Sensitivity of Near-Infrared Permanent Laser Scanning Intensity for Retrieving Soil Moisture on a Coastal Beach: Calibration Procedure Using In Situ Data. *Remote Sens.* **2021**, *13*, 1645. [[CrossRef](#)]
73. Zahiri, Z.; Laefer, D.F.; Gowen, A. Characterizing Building Materials Using Multispectral Imagery and LiDAR Intensity Data. *J. Build. Eng.* **2021**, *44*, 102603. [[CrossRef](#)]
74. Bowyer, P.; Danson, F.M. Sensitivity of Spectral Reflectance to Variation in Live Fuel Moisture Content at Leaf and Canopy Level. *Remote Sens. Environ.* **2004**, *92*, 297–308. [[CrossRef](#)]
75. Paltridge, G.W.; Mitchell, R.M. Atmospheric and Viewing Angle Correction of Vegetation Indices and Grassland Fuel Moisture Content Derived from NOAA/AVHRR. *Remote Sens. Environ.* **1990**, *31*, 121–135. [[CrossRef](#)]
76. Wade, D. Fuel Moisture and Prescribed Burning. *South. Fire Exch. Fact Sheet* **2013**, *5*, 5–8.
77. Zhu, X.; Wang, T.; Darvishzadeh, R.; Skidmore, A.K.; Niemann, K.O. 3D Leaf Water Content Mapping Using Terrestrial Laser Scanner Backscatter Intensity with Radiometric Correction. *ISPRS J. Photogramm. Remote Sens.* **2015**, *110*, 14–23. [[CrossRef](#)]
78. Kaasalainen, S.; Krooks, A.; Kukko, A.; Kaartinen, H. Radiometric Calibration of Terrestrial Laser Scanners with External Reference Targets. *Remote Sens.* **2009**, *1*, 144–158. [[CrossRef](#)]
79. Li, Y.; Duthon, P.; Colomb, M.; Ibanez-Guzman, J. What Happens for a ToF LiDAR in Fog? *IEEE Trans. Intell. Transp. Syst.* **2021**, *22*, 6670–6681. [[CrossRef](#)]
80. Strand, M.P.; Witherspoon, N.H.; Holloway Jr, J.H.; Tinsley, K.R.; Petee, D.A.; Taylor, J.S., Jr.; Branham, E.A.; Thomas, J.P. Environmental Factors Impacting the Performance of Airborne Lidar Sensors in the Surf Zone. In Proceedings of the Detection and Remediation Technologies for Mines and Minelike Targets VIII, Orlando, FL, USA, 21–25 April 2003; SPIE: Bellingham, WA, USA, 2003; Volume 5089, pp. 274–283.
81. Levy, J.S.; Johnson, J.T.E. Remote Soil Moisture Measurement from Drone-Borne Reflectance Spectroscopy: Applications to Hydroperiod Measurement in Desert Playas. *Remote Sens.* **2021**, *13*, 1035. [[CrossRef](#)]

Disclaimer/Publisher’s Note: The statements, opinions and data contained in all publications are solely those of the individual author(s) and contributor(s) and not of MDPI and/or the editor(s). MDPI and/or the editor(s) disclaim responsibility for any injury to people or property resulting from any ideas, methods, instructions or products referred to in the content.